LLNL-JRNL-837400

LH2 Storage System for Heavy Duty Trucks:Configuration, performance, cost, and safety

S. M. Aceves, N. J. Killingsworth, H. S. Roh, J. K. Peng, R. K. Ahluwalia, J. A. Ronevich, C. Houchins

July 13, 2022

International Journal of Hydrogen Energy

Liquid Hydrogen Storage System for Heavy Duty Trucks: Configuration, Performance, Cost, and Safety

R. K. Ahluwalia [a], H-S Roh [a], J-K Peng [a], D. Papadias [a], A. R. Baird [b], E. Hecht [b], B. D. Ehrhart [b], A. Muna [b], J. A. Ronevich [b], C. Houchins [c], N. J. Killingsworth [d], S. M. Aceves [e,*]

[a]Argonne National Laboratory, 9700 S. Cass Avenue, Lemont, IL 60439

[b]Sandia National Laboratories, 1515 Eubank Blvd SE, Albuquerque, NM 87123

[c]Strategic Analysis, Inc., 4075 Wilson Boulevard Arlington, VA 22203

[d]Lawrence Livermore National Laboratory, 7000 East Ave, Livermore, CA 94550

[e]National Technological Institute of Mexico, Celaya, Mexico

Abstract

We investigate the potential of liquid hydrogen storage (LH_2) on-board Class-8 heavy duty trucks to resolve many of the range, weight, volume, refueling time and cost issues associated with 350 or 700-bar compressed H_2 storage in Type-3 or Type-4 composite tanks. We present and discuss conceptual storage system configurations capable of supplying H_2 to fuel cells at 5-bar with or without on-board LH_2 pumps. Structural aspects of storing LH_2 in double walled, vacuum insulated, and low-pressure Type-1 tanks are investigated. Structural materials and insulation methods are discussed for service at cryogenic temperatures and mitigation of heat leak to prevent LH_2 boil-off. Failure modes of the liner and shell are identified and analyzed using the regulatory codes and detailed finite element (FE) methods. The conceptual systems are subjected to a Failure modes and effects analysis (FMEA) and a safety, codes, and standards (SCS) review to rank failures and identify safety gaps. The results indicate that the conceptual systems can reach 19.6% usable gravimetric capacity, 40.9 g-H_2/L usable volumetric capacity and \$174-183/kg-H_2 cost (2016 USD) when manufactured 100,000 systems annually.

1 Introduction

Liquid hydrogen's (LH_2) high density (71 kg/m^3) at ambient pressure is a major advantage that makes liquefaction the preferred approach to distribute and store H_2 throughout the infrastructure despite the high energy and cost of liquefaction and its propensity to boil-off during storage and transfer [1].

Automotive LH_2 technology was developed in the last century by many manufacturers including BMW. Starting at a time when composite pressure vessel technology had not fully matured, the effort produced practical automobiles and achieved a range comparable to gasoline vehicles by storing up to 13 kg of LH_2 in cryogenic vessels with vacuum multilayer insulation (MLI) [2]. The effort led to the production of 100 LH_2 vehicles and evaluation of cost-effective approaches to mass production [3] [4].

Despite the advantages and promise of LH_2 automobiles, they face a major challenge: the extreme sensitivity of LH_2 to heat transfer from the environment, resulting in rapid pressurization potentially leading to vent losses if the vessel maximum allowable pressure is reached and the relief device opens [5].

It is possible to avoid vent losses in LH_2 automobiles. However, this requires sufficient driving to consume evaporated LH_2 before the vessel pressurizes to the relief device setting. In practice, this is a challenge because (1) many personal vehicles are infrequently used, remaining parked for days or even weeks, and (2) even the best MLI is challenged to reduce heat transfer to the necessary level due to the relatively small capacity (~10 kg H_2) of automotive LH_2 vessels leading to large surface area to volume ratios.

The challenge of avoiding large LH_2 losses, along with the maturity of composite vessels for high pressure gaseous hydrogen (GH_2) [6], and the development of cryo-compressed H_2 storage technology as a high-density alternative to LH_2 storage with reduced sensitivity to heat transfer [7], led to the (possibly temporary) demise of LH_2 automobiles.

Recent emphasis in the development of zero emissions H_2-fueled heavy trucks [8] has, however, renewed interest for low-pressure LH_2 vessels for mobile application. Frequent utilization and the large amount of hydrogen necessary for practical truck usage can reduce the sensitivity to heat transfer to a level where vent losses can be eliminated under typical driving scenarios. Even if vent losses may still occur during long periods of inactivity (days), these are expected to be infrequent and contribute little to the truck cost of ownership. Applicability of LH_2 in the aviation field is also being considered for reduced environmental pollution and CO_2 emissions [9] [10] [11], with similar advantages in terms of mitigated vent losses due to rapid utilization and large vessel dimensions.

This paper analyzes the structural, systems, economics, and safety issues of LH_2 storage and utilization onboard trucks. Vessel location within the truck is first discussed, followed by vessel structural design and analysis. System gravimetric (H_2 weight %), volumetric (grams of H_2 per liter of system volume), and cost (\$/kg-H_2) storage performances are calculated based on usable H_2 storage capacity determined in a companion paper [12] as the amount of H_2 that can be stored while still meeting dormancy constraints. The paper concludes with a safety analysis and a description of existing codes applicable to LH_2-fueled trucks.

1.1 LH_2 vs. LNG

Liquefied natural gas (LNG) has a growing importance as a fuel for heavy trucks. Cost reduction mainly due to non-conventional extraction (fracking) in the United States has made natural gas a very economical alternative for power generation as well as transportation [13].

LNG has environmental in addition to economic advantages: clean combustion of LNG causes nearly 99% less particle matter (PM) and sulfur oxide (SOx) emissions, and around 80% less nitrogen oxides than diesel fuel [14]. CO_2 emissions are also lower than for diesel engines by ~20%, although this advantage may be partially offset by methane leaks since methane's impact on climate change is 25X greater than the same mass of CO_2 over a 100-year period [15]. Minimization of natural gas leakage into atmosphere during fueling and storage is crucial [16].

Economic and environmental advantages have resulted in increased utilization of LNG in heavy trucks. The United States currently has 58 public LNG filling stations across the country [17], and China is world leader with more than 230,000 LNG trucks and around 3000 filling stations (CNG and LNG) [18].

Considering the widespread and rapidly growing utilization of LNG as a fuel for heavy trucks, it is worthwhile to contrast the physical characteristics of LH_2 vs. LNG and evaluate the advantages and challenges that may guide the effort toward practical heavy-duty trucks fueled with LH_2.

Table 1 shows key physical parameters that may affect practical implementation of LH_2 and LNG as a fuel for heavy-duty trucks. LH_2 has lower storage temperature, resulting in increased heat transfer rate for given insulation quality. Combined with LNG's higher heat of vaporization, we can conclude that LH_2 is more sensitive to environmental heat transfer, potentially leading to more abundant vent losses under infrequent driving scenarios.

LNG has a major density advantage (>6X larger kg/L) which is partially offset by LH_2's greater heating value, so that LNG's chemical energy density (kWh/L) is 2.64X that of LH_2. This still rather large difference in energy density can be somewhat mitigated by the higher efficiency of H_2 fuel cells at 60% peak efficiency [19] vs. NG spark ignited internal combustion engines at 38% peak efficiency [20]. Ultimately, the lower energy density is expected to increase vessel cost and could reduce the range of LH_2 vs. LNG trucks. Determining whether LH2 trucks can still be practical despite reduced energy density demands a detailed analysis and is the subject of this and the companion paper [12].

The very low ignition energy and rapid flame speed of H_2 have implications for LH_2 vehicle safety [21]. However, this propensity to ignite is mitigated by the low H_2 density resulting in large buoyancy and rapid diffusion. Rapid flame speed represents an advantage for hydrogen-fueled spark-ignited engines [22] when these find application in heavy-duty vehicles, possibly due to durability and cost advantages vs. fuel cells.

Despite some advantages of LNG, LH_2 is ultimately the preferred option because it can be produced and consumed without CO_2 or regulated emissions, providing a near-term alternative for zero emissions heavy-duty transportation without the weight, volume, cost, and recharging constraints of today's electric batteries. However, practical solutions to LH_2 dispensing and onboard storage need to first be demonstrated.

2 Cryogenic Vessel Analysis

Storage of liquid hydrogen for transport applications requires a well-insulated vessel to prevent phase change by minimizing heat transfer from the outside. When LH_2 vaporizes, the pressure inside the vessel increases, and release of gaseous H_2 can become necessary to remain below the maximum allowable pressure. In order to minimize heat transfer, the cryogenic vessel is composed of three parts. As shown in Fig. 1, an inner liner stores LH_2, a shell protects the inner liner and provides connections with external structures, and a multilayer insulation (MLI) minimizes radiative and convective heat transfer to the liner. A vacuum is maintained in the space between the liner and the shell to minimize conductive and convective heat transfer through the remaining gas that fills the voids between the MLI.

2.1 Vessel Configurations

Taking the lead from compressed natural gas (CNG) industry, three locations where LH_2 vessels can be mounted on a truck were considered based on currently available retrofit options: (1) Frame Mounted (FM), (2) Roof Mounted (RM), and (3) Behind the Cab (BTC). The size and number of vessels that can be installed depend on the truck platform and the storage location. Following the packaging options offered by A-1 Alternative Fuel Systems for CNG, Table 2 shows storage systems with two vessels for FM, four vessels for RM, and 2-4 vessels for BTC. Additionally, two thicknesses of liner separation are investigated, 11 mm and 21 mm. Among these options, the available CNG storage capacity (i.e., internal volume of the vessel array) is the largest for FM configuration 10 with 66-cm outer diameter (D_o), 305-cm outside length (L_o) and 11 mm of liner separation. This configuration is of particular interest and has been selected for detailed analysis as it may help define the maximum achievable range for class-8 trucks with on-board LH_2 storage. It may also help identify the smallest specific storage cost (\$/kg-H_2) because many system components (valves, safety devices, pumps, etc.) have fixed costs independent of storage capacity, and their impact on marginal H_2 storage cost drops as capacity increases. In our analysis, we consider that the packaging envelope limits the outside length and diameter and determine the available storage volume for LH_2 after calculating the volume occupied by the shell, vacuum insulation, and liner.

2.2 Materials

Due to the low temperatures (~20 K) required to keep hydrogen in a liquid state, the structural materials available for use in LH2 storage applications are limited. Conventional lower-cost, ferritic steels which are used in high-pressure gaseous hydrogen storage up to 1000 bar are not likely candidates due to the ductile-to-brittle transition temperatures (DBTT) of these alloys occurring at temperatures above 20 K. The DBTT refers to a significant drop in toughness with decreasing temperature. Some cryogenic steels such as 9%Ni steels are rated for use down to 77 K which work well in LNG applications where storage temperatures are 111 K. However, these materials are not conventionally used with LH_2 either due to lack of data at 20 K or incompatibility with hydrogen. Therefore, the conventional materials that are used for storing liquid hydrogen are austenitic stainless steels (304 and 316) where no real DBTT exists, and the material maintains adequate mechanical properties down to 20 K. The other alternative material class is aluminum alloys which also exhibit a lack of DBTT but have overall lower fracture toughness and ductility compared to austenitic stainless steels.

The other aspect of materials selection for on-board liquid hydrogen applications that needs to be considered is the material's susceptibility to hydrogen embrittlement, in which mechanical properties can be degraded due to the presence of hydrogen. Fortunately, many of the materials that perform well at low temperatures are also suitable with hydrogen (e.g., austenitic stainless steels, aluminum alloys). At room temperature, hydrogen does degrade the mechanical properties of austenitic stainless steels; however, the fracture toughness of the austenitic stainless steel is quite high such that even with a reduction in fracture toughness, the structural integrity is often not compromised. Due to the challenges in performing in-situ experiments in liquid hydrogen, limited mechanical property measurements have been made in this environment to evaluate the extent of hydrogen embrittlement at liquid hydrogen temperatures. The phenomenon of hydrogen embrittlement is a kinetically driven process in that hydrogen must be able to diffuse into the material and interact with regions of elevated stress in order to cause embrittlement. Since diffusion is a thermally activated process, low temperatures greatly reduce hydrogen diffusion into the material suggesting that embrittlement due to hydrogen may be reduced. It is likely that the low temperature may have a more dominant effect than hydrogen.

Selection of material for use in liquid hydrogen storage is influenced not only by the factors mentioned above (e.g., temperature and hydrogen embrittlement susceptibility) but also from cost and design constraints (stresses, pressure cycling, weight). In a cryo-compressed system, the wall thickness would need to be sufficient to withstand higher pressures compared to a liquid hydrogen system operating at nominally atmospheric pressures. Aluminum alloys provide significant weight savings but also have lower strength and fracture toughness than austenitic stainless steels which would require larger thicknesses to keep wall stresses down. Within the class of austenitic stainless steels, 304 and 316 are the traditional materials of choice for liquid hydrogen storage. However, nitrogen-strengthened austenitic alloys offer potential cost savings due to the ability to attain higher strengths along with lower cost alloying additions which could potentially be used for liquid hydrogen storage.

Table 3 lists the mechanical properties and density of the four structural materials considered in this study. Along with ultimate strength and yield stress, fracture toughness is a key mechanical property since it is a measure of the resistance to the propagation of cracks and hence the endurance of a material to stress cycles. In general, but not always, metals have increased ultimate and yield strengths as the operating temperature decreases. Aluminum 5083 is the most frequently used material at cryogenic temperatures although aluminum 2219 has been used as a vessel material for storing cryogenic liquid fuel in launch vehicles. Austenitic stainless steels such as SS304 and SS316 are also used for cryogenics because they have excellent strength and fracture toughness even at low temperatures. As listed in Table 3, the allowable stress increases by 52% for Al 2219, 36% for Al 5083, and 77% for SS 304 when these materials are cooled from ambient temperature down to -195°C.

Multi-layer insulation (MLI) is a preferred method for cryogenic steel tanks with vacuum jackets and is capable of limiting heat gain to 1-2 W/m^2. Vacuum jackets with perlite powder or glass bubble insulation systems are used in stationary applications for very large LH_2 storage tanks. The MLI system consists of alternating layers of reflector and spacer materials. The critical factors in MLI selection are the level of vacuum, vacuum stability, number of insulation layers and insulation thickness. Structural support is another important material that determines the heat leak. In this work, we selected MLI with 1-1.5 mTorr vacuum, 11- or 21-mm layer thickness, and G-10 support. Alternate methods such as layered composite insulation (LCI) systems and aerogel composite blankets have also been investigated.

2.3 Shell Buckling

Since the shell is exposed to atmospheric pressure on the outside and vacuum on the inside, buckling is the main failure mode. We consider that the shell domes are semielliptical with an axial length equal to 1/4th of the cylinder diameter.

ASME BPVC Section VIII Division 1 and Section II, Part D, and Subpart 3 specify a method to determine the minimum shell thickness in terms of two factors, *A* and *B*, that depend on the geometry and material. Factor *A* is obtained from the ratio of the design length to outer diameter of the shell and the ratio of the diameter to thickness. The design length is measured between lines of supports as seen in Fig. 2. A line of support is defined as a circumferential line on a dome at one-third the depth of the dome from the dome tangent line. Stiffening rings, if present, can also be lines of support.

Factor *B* is determined from factor *A* and a chart for the material to be used. While this chart is not available for Aluminum 2219, we observe that, for the vessel geometry being considered and for many similar aluminum denominations, factor A falls in the linear region of the chart. It is therefore possible to estimate factor B from factor *A* and Young's modulus *E* according to the following equation,

$$B = \frac{AE}{2} \tag{1}$$

The allowable external pressure can be calculated from Eq. (2) using an initially estimated value of shell thickness, *t*, and the outer diameter of the shell, along with the previously obtained factor *B*. If the allowable external pressure is higher than the criteria pressure of 103 kPa (P_a), the proposed shell thickness can be used. Otherwise, it is necessary to increase the thickness of the shell or add stiffening rings to avoid shell buckling failure.

$$P_a = \frac{4B}{3(D_o/t)} \tag{2}$$

Adding a stiffening ring to the shell can increase the critical buckling load and reduce the required shell wall thickness. ASME BPVC also provides design guidelines for shells with stiffening rings. The moment of inertia (I_s) of the stiffening ring is calculated from the following equation.

$$I_s = [D_0^2 L_s(t + A_s/L_s)A]/14 \tag{3}$$

where L_S is half of the distance between support lines and A_S is the cross-sectional area of the stiffening ring. We consider that the stiffening ring is made of the same material as the shell, is 6-mm wide and 50-mm high. This stiffening ring is welded to the center of the shell in the circumferential direction. In the buckling analysis of a LH_2 vessel with the stiffening ring, factor B is first calculated from Eq. (4) below, and then factor A is obtained from Eq. (1) because the ASME Code does not include a chart for aluminum 2219.

$$B = \frac{3}{4}\left(\frac{PD_O}{t + A_S/L_S}\right) \tag{4}$$

We also conducted a linear buckling analysis by creating a FE model in ABAQUS. Since the cryogenic vessel has a large diameter to thickness ratio, the FE model was created using shell rather than the solid elements. For boundary conditions, one end is considered fixed, and the other end is allowed to move in the axial direction.

2.4 Liner Burst

The liner contains LH_2 at 20-30 K and both ends of the liner are suspended by brackets attached to the shell. Liner wall thickness is calculated to sustain 10 bar maximum allowable pressure. Although the liner contains cryogenic LH_2, lower material strength at ambient temperature is used in the stress analysis because the liner could be pressure tested or operated at room temperature. The liner uses elliptical domes with a length equal to 1/4th of the diameter.

Liner thickness is determined to withstand the hoop stresses due to internal pressure. Other loads exist, such as the vessel weight, dynamic loads (e.g., from road and driving conditions), cyclic pressure load from filling and emptying, and thermal loads from temperature distributions and differential thermal expansion, but these are negligible compared to the loads created by the internal pressure.

The outer liner diameter is calculated by subtracting the shell and MLI thicknesses from the outer shell diameter. According to ASME BPVC Section VIII Division 1, the thickness of the cylindrical part of the liner can be calculated as,

$$t = \frac{PR}{\eta\sigma_a - 0.6P} \tag{5}$$

where,
P = maximum allowable internal design pressure
R = inner radius of the liner
σ_a= maximum allowable stress

η = joint efficiency
t = minimum required liner thickness

Joint efficiency for liner sections connected by welds is a function of the welding and inspection method. In this study, a joint efficiency of 0.9, as recommended for full single-welded butt joint with a backing strip, is conservatively applied.

The liner is also modeled with static FE analysis using shell elements and a thickness obtained from Eq. (5), to check that stresses are within allowable limits. Due to the geometrical complexity, elliptical shape and a hole for the boss port, the dome thickness is also determined from FE analysis. FE analysis considers aluminum 2219, but other materials (aluminum 5083 and stainless steel 304) are also modeled to compare their performance.

2.5 LH_2 Sloshing

Heavy-duty trucks undergo various levels of accelerations and decelerations while driving. Although trucks store relatively small amounts of LH_2 when compared to fuel tankers, the motion of LH_2 in the vessel increases loads on vessel walls, creates viscous heating, and may create instability. We simulate the sloshing of LH_2 inside a half-filled vessel using a Coupled Eulerian-Lagrangian (CEL) method provided in ABAQUS [23] for modeling fluid-structural interactions. CEL is considered superior to the traditional Lagrangian method in which the material points are fixed to the nodes and the motion of the nodes determines deformation and stress; remeshing is needed resulting in numerical inaccuracies and long computational time. In the Eulerian method, mainly used in computational fluid dynamics (CFD), the mesh is fixed, and the material moves through it. An Arbitrary Lagrangian-Eulerian (ALE) method resolves some of the issues in the Lagrangian method by providing for an independent movement of the mesh and material. The CEL method has the advantage over ALE in that the non-translating Eulerian material interacts with the deforming Lagrangian elements making it particularly suitable for fluid-structural interaction simulations such as sloshing and excessive deformation. Recent numerical analysis of sloshing [24] was performed on a LH_2 tank under sinusoidal excitation.

We performed the sloshing analysis of a half-filled liner using ABAQUS/Explicit to investigate LH_2 motion and the hydrodynamic impact load exerted on the liner during sudden deceleration. Sloshing analysis assumes 2 m/s initial truck speed, 2g deceleration, and 0.1 s stopping time. The process is modeled for 0.8 s, and the Eulerian domain is specified to include all motion of the liner. The effect of a baffle inside the liner is also investigated to evaluate the potential to mitigate slosh and reduce hydrodynamic impact loads. We assume that the baffle thickness is equal to the liner thickness and the height is ~10% of the liner diameter.

3 Results and Discussion

3.1 Two-vessel Fuel Systems

3.1.1 Storage system with Pump

Fig. 3 presents a schematic of the onboard fuel storage system with two vessels connected to a common external LH_2 pump. A simpler but costlier alternative is to have separate submerged internal LH_2 pumps and avoid the possible issues of priming and cavitation. Each vessel is equipped with an integrated valve assembly that houses a pressure transducer, safety valves, control valves, an excess flow valve and a check valve.

During refueling, LH_2 is fed to the vessels from the fill receptacle through the tubes marked in green. A top-fill configuration is shown but a bottom-fill configuration is also feasible. Each vessel has a liquid level sensor to monitor the amount of H_2 in the tank and to prevent overfill by tripping the control valves CV2 or CV5. Fast and complete refueling is enabled by venting gaseous H_2 (GH_2) through a vent tube if the tank pressure rises above a preset level. It is desirable and possible to return the vented H_2 to the refueling station where it may be reliquefied or compressed and used for other purposes.

During truck operation, LH_2 is pumped from the cryogenic vessel (red line) and enters the vaporizer where it is converted to gas on its way to the fuel cell stack. If the vessel pressure exceeds the minimum fuel cell feed pressure, GH_2 can be fed to the fuel cell (black line) directly from the vessel. When possible, extraction of GH_2 is preferred as it depressurizes the vessel and extends dormancy.

The boss section has three penetrations for LH_2 refueling, LH_2 discharge and GH_2 venting. GH_2 may be vented to the refueling station during refueling, directly discharged to the fuel cell during vehicle operation, or vented to the environment through the safety valves SV1 or SV2 if the vessel pressure exceeds the allowable limit (e.g., during periods of extended inactivity).

3.1.2 Storage System without Pump

Fig. 4 presents a schematic of a fuel storage system without an on-board LH_2 pump. In this system, the storage vessels must always be maintained above the target 5-bar fuel cell inlet pressure. During refueling, LH_2 has to be fed at a pressure above 5 bar and may have to be preheated to prevent the vessel pressure from dropping below 5 bar. Some heat also needs to be supplied during truck operation to compensate for the drop in vessel pressure as the stored LH_2 is extracted and fed to the fuel cell. This is accomplished in Fig. 4 by vaporizing the extracted LH_2, circulating a portion of the vaporized H_2 through an in-tank heat exchanger (purple line), and remixing it with the gas flowing to the fuel cell. A flow divider valve and two check valves are incorporated in Fig. 4 to control the fraction of vaporized H_2 that is circulated.

Absence of an on-board LH_2 pump impacts the system performance in several ways. Compared to the system with an on-board pump, the storage capacity is smaller because at a higher storage temperature (e.g., the saturation temperature corresponding to 5 bar), LH_2 density is lower. Maintaining >5 bar storage pressure requires heating of LH_2 feed during refueling and stored LH_2 during discharge. This heating is a conceptual contradiction to providing a vacuum insulation around the liner to mitigate heat ingress from the ambient. Dormancy is also reduced due to the smaller differential between the storage and maximum allowable pressures. Nevertheless, removing the on-board pump simplifies the system configuration and may recover the storage volume otherwise occupied by an internal pump.

3.2 Shell

Using the ASME BPVC method described in Section 2.3, we calculate the required thickness of an aluminum-2219 shell as 5.8 mm. Fig. 5a shows the buckling behavior of this shell modeled by the FE analysis method also described in Section 2.3. The observed deformation pattern consists of three waves. In general, the longer the cylinder length, the smaller the number of waves and the lower the critical buckling load. The FE model indicates that the shell domes are only required to be half as thick as the cylindrical part, resulting in a total shell weight of 99.4 kg. Also, the critical external pressure is 309 kPa for an overall safety factor of 3 for shell buckling.

The critical buckling load depends mainly on the geometry of the structure and the stiffness of the material. The ASME BPVC method indicates that adding a 6-mm wide and 50-mm high circumferential stiffening ring reduces the required shell thickness in the cylindrical section to 2.9 mm (see Table 4). Fig. 5b shows the buckling behavior of the shell from the FE model with the stiffening ring and the change in the deformation pattern to one with four waves. Including the ring, the shell weighs 78 kg and is 21.5% lighter than without the ring.

3.3 Liner

Liner thickness is calculated using the ASME BPVC Section VIII Division 1 method for the three materials being considered. Of the three materials, stainless steel has the highest allowable strength but also the highest density whereas aluminum 2219 has the same density but higher allowable stress than aluminum 5083. Within the fixed packaging envelope defined by the shell outer dimensions, subtracting the shell and insulation thickness and allowing space in the head annulus for liner support, coils, and plug, we estimate the liner outer diameter as 62.1 cm and outer length as 281.5 cm. As shown in Table 5, the liner calculated from the ASME code is thinnest but heaviest for stainless steel and thickest for aluminum 5083. An aluminum 2219 liner has the lowest weight due to its high strength and low density. A liner made of aluminum 5083 is about 70% heavier than one made of aluminum 2219.

Fig. 6 shows the stress distribution calculated from the FE model for an aluminum 2219 liner that is 2.7-mm thick in the cylindrical section and has an elliptical dome with an opening for each end port. The stress concentration at the junction between the dome and the cylindrical sections is of particular concern. We have iteratively determined that the principal stresses in the dome are within allowable limits if the dome thickness varies between 2.9 mm at the junction with the cylinder and 4.5 mm at the port. As expected, the principal stress is highest in the cylindrical section, nearly uniform, and close to the maximum allowable stress for an overall safety factor of 3.5.

3.4 LH_2 Sloshing

Fig. 7 shows LH_2 sloshing motion in a half-filled vessel without (left) and with (right) a baffle when the truck decelerates at 2g from an initial speed of 2 m/s, stopping after 0.1 s. As time advances, LH_2 moves forward (to the right) due to inertia and contacts the upper part of the liner by 0.2 s. The baffle restricts the forward flow and assists in rapidly stabilizing sloshing compared to the case without a baffle.

Fig. 8 depicts von Mises stress distribution on the liner at 0.1 s. The stress is caused by a combination of deceleration and LH_2 sloshing. The maximum stress occurs near the junction between the cylinder and the dome, and very low stresses are observed in the baffle. The stress levels are negligible compared to the yield strength of the metal (100-300 MPa). However, further analysis is necessary for larger vessels (e.g., LH_2 tanker trucks) to determine whether sloshing may affect maneuvering stability.

3.5 System Conceptualization and Performance

Fig. 9 shows the conceptual LH_2 fuel system for heavy duty trucks. In the selected configuration, LH_2 vessels are mounted on each side of the frame. The (aluminum 2219) liner is suspended inside the (aluminum 2219) shell by means of a support bracket that is welded to the shell and the liner port. The conceptual system includes three tubes for refueling, extracting LH_2, and extracting GH_2. Since these tubes are directly connected to the liner, their length is maximized by coiling them inside the vacuum space in between the liner and shell to reduce heat transfer.

The liner and shell have three-part construction using hydraulic rolling, progressive roll forming or stretch forming for the cylinder, deep drawn forming for the domes, and butt welding for joining the liner with domes. The dome forming method allows for variable thicknesses and port opening. The tank balance of plant (BOP, one per tank) includes the integrated valve assembly, fuel spraying nozzle, liquid level transducer, rupture discs and holders, and boss and plug. The system BOP (one per system) includes the fill receptacle, discharging receptacle, diverter valve, check valve, safety valve, drain valve, pressure transducer, tubes, and fittings, LH_2 pump, and vaporizer heat exchanger.

Fig. 10 presents the volumetric and gravimetric capacities for the LH_2 storage system defined based on usable H_2. Inclusive of the weights and volumes of all components, the system has 22.8% H_2 weight fraction, out of which 19.6% are usable, i.e., can be discharged within the pressure and flow rate requirements of the truck fuel cell. Usable volumetric capacity is 40.9 kg/m^3. The stored hydrogen occupies 77% of the total volume, followed by insulation at 9% and tank BOP at 8%. Thin structural components, liner and shell, account for < 5% of the system volume but a major fraction (64.6%) of the system weight. Other significant contributors to the system weight are tank and system BOP at 12.3%.

At 40.9 kg-H_2/m^3 system volumetric capacity, the frame mounted configuration with two vessels stores 86.8 kg of usable H_2. If a fuel cell system for Class-8 heavy duty trucks achieves a fuel economy of 7.6-8.5 miles/kg-H_2 on a truck relevant duty cycle, we calculate a range of 660-738 miles (1060-1187 km) between consecutive refuelings. Although this is somewhat less than available in today's diesel or LNG-fueled trucks, it may be sufficient to meet most driving requirements of heavy-duty trucks.

3.6 Cost Analysis

Factory costs are projected for the 10 vessel packaging options considered in this paper and shown in Table 2. Factory costs include capital equipment costs, labor, energy costs, and materials but do not include margins as described, for example, in [25]. Manufacturing assumptions—process flow, cycle times, and material inputs—were adapted from Lasher [26] and updated to account for larger vessels and differences in system design. Pump costs are based on designs in [27] and discussions with pump suppliers. These include different numbers of vessels and locations: roof-mounted, behind-the-cab, and frame-mounted (Section 2.1). In addition to this, two MLI thicknesses are considered (11 and 21 mm), and inner volumes are calculated for each of the 10 packaging options and two MLI thicknesses. All factory costs are reported in 2016$ and projected to production rates of 100,000 systems annually to allow direct comparison with published U.S. Department of Energy targets [28]. Table 6 summarizes the projected system cost ($/kg of usable H_2), total system mass, and usable H_2 capacity for each of the configurations and insulation thicknesses considered. H_2 usable storage capacities are calculated in a companion paper [12], and represent the H_2 mass that can be extracted from the vessels while meeting fuel cell feed pressure demands and dormancy constraints.

Fig. 11 presents the same data as stacked bars to compare the split between vessel and balance of plant costs. Fig. 12 shows a full cost breakdown by component for configuration 10 (frame-mounted, two vessel system with 11 and 21 mm MLI) selected early in the paper for detailed analysis due to its large capacity (86.8 and 89.1 kg H_2).

It is observed from Table 6 and Fig. 11 that configuration 10 has a major cost advantage (174-183 $/kg of usable H_2) in addition to a storage capacity advantage when compared to other configurations. As previously noted, this is primarily due to balance of plant scaling: for systems with the same number of vessels but different capacity (e.g., configurations 4 and 10), the balance of plant cost are nearly equal (~$10,000 for both), but the capacity of configuration 10 is about 4X that of configuration 4. Some balance of plant components are duplicated for each vessel (e.g. spray nozzle, control valves, rupture discs). The balance of plant is ~$14,500 for a 4-vessel system compared with $10,000 for a 2-vessel system (e.g., configurations 3 vs. 5) due to component duplication.

3.7 Safety Codes and Standards

The proposed heavy-duty vehicle liquid hydrogen fuel system with and without an onboard pump (Fig. 3 and Fig. 4) were carefully analyzed for safety according to a failure modes and effects analysis (FMEA) to identify and qualitatively rank failures that could result in a leak or release of either gaseous or liquid hydrogen.

A failure mode defines how a component fails whereas a failure cause describes scenarios postulating why a component failed. The primary focus of this FMEA was to identify the credible scenarios and failure modes that could lead to either a leak or release of GH_2 or LH_2. A failure mode can either be an operation, function, or status of a component. The failure effects are a direct consequence of the failure mode.

The FMEA results have been published separately [29]. Only low and medium risks were identified. A high-risk failure would lead to a catastrophic release of LH_2 and GH_2 occasionally, or an unintended frequent release of GH_2, neither of which were identified. Overall, the main two differences in the medium risk failures between the two systems comes from the flow diverter present in the system without an onboard LH2 pump.

For the system with an onboard LH_2 pump, a total of 14 failure modes with medium risk priority were identified. These 14 failure modes can fall within 3 categories: cryogenic vessel failures (2 identified), failures of valve/pressure relief device (3 identified), and failures involving hardware (9 identified). For the system without an onboard LH_2 pump, a total of 16 failure modes with medium risk priority were identified: cryogenic vessel failures (2 identified), failures of valve/pressure relief device (5 identified), and failures involving hardware (9 identified). Failure of the cryogenic vessel is improbable but leads to a large release of both GH_2 and LH_2. Valve and pressure-relief failures can lead to both leakage of GH_2 and/or LH_2. Failure of hardware includes incorrect pressure measurements and pump speeds leading to incorrect operation which might over-pressurize part of the system. Additionally, the vaporizer could develop a leak in one of the coils leading to a release of GH_2 or LH_2.

A safety, codes, and standards (SCS) review was also conducted. The intent of this review was to identify safety gaps, missing components, and determining where improvements can be made. The review inspected the following three Society of Automotive Engineers (SAE) Standards/Recommended Practices:

- SAE J2343- Recommended Practices for LNG Powered Heavy-Duty Trucks [30]
- SAE J2578- Recommended Practice for General Fuel Cell Vehicle Safety- Liquid or Heavy Duty Specific [31]

- SAE J2579- Standard for Fuel Systems in Fuel Cell and Other Hydrogen Vehicles- Liquid or Heavy Duty Specific [32]

Additionally, National Fire Protection Association (NFPA) 52- Vehicular Natural Gas Fuel Systems Code 2019 Edition [33], Section 16.4 LNG Engine Fuel Systems was used during the LH_2 fuel system review. While NFPA 52 and SAE J2343 are specific for natural gas systems, there are some relevant practices that can be applied to HDV LH_2 fuel systems. Detailed results of the review have been published in a separate report [29].

The SCS review identified that any vehicle design will need to ensure that valve and pressure relief configurations are designed to prevent trapping of fuel in various parts of the system. Additionally, spaces where fuel will be trapped such as when fueling is complete must have pressure relief devices. Both the system with the pump and with the pressure build loop were found to have some areas that require pressure relief devices due to the potential for trapped fuel. Additional detail would be necessary for a comprehensive evaluation of the integrated valve assembly box. All recommendations from the SCS review have been incorporated into the system diagrams (Fig. 3 and Fig. 4).

4 Summary and Conclusions

This paper considers the practical applicability of LH_2 storage systems for heavy-duty trucks. In combination with a companion paper [12], potential systems for LH_2 storage and delivery are modeled to establish necessary vessel wall and insulation thicknesses to determine system cost as well as volumetric and gravimetric performance. Codes and standards are considered for evaluation of system design and devices necessary for future truck application. The main conclusions obtained from the analysis are as follows.

1. An arrangement of dual frame-mounted vessels (Fig. 9 and Configuration 10 in Table 2) is selected among the many alternatives because of its highest capacity leading to the longest vehicle range and lowest cost per kg of usable LH_2 storage.
2. Aluminum 2219 is identified as a promising onboard LH_2 tank material for both the liner and shell, owing to its low density as well as its strength and toughness. Structural analysis based on the ASME boiler and pressure vessel code [34] as well as FE analysis reveals the necessary liner and shell wall thicknesses. These thicknesses, along with estimated weights for balance of plant components, are used for determining system gravimetric storage performance (H_2 weight %). A very promising result of 19.6% H_2 usable weight fraction indicates potential for light LH_2 storage vessels with minor impact on overall truck weight and cargo capacity.
3. A volumetric capacity of LH_2 storage at 40.9 grams of usable H_2 per liter of system volume, including vessels and balance of plant, results in 86.8 kg of usable H_2, sufficient for 1,057 km (660.4 mile) of range in a heavy-duty truck with 12.2 km/kg H_2 (7.61 mile/kg H_2) fuel

economy. Although this is less than available in today's diesel or LNG-fueled trucks, it may be sufficient to meet most daily driving requirements of heavy-duty trucks.

4. A system cost of \$174 per kg of usable H_2 (11 mm thick insulation) or \$183 per kg of usable H_2 (21 mm thick insulation, Table 6) results in \$15,088 - \$16,268 total system costs for configuration 10 (Table 2 and Fig. 10). While these costs are higher than for diesel and LNG trucks, they do not add considerably to the total truck cost and offer the promise of practical zero emission heavy-duty truck propulsion.
5. The proposed system configurations have been carefully reviewed and modified for compliance with codes and standards relevant to LH_2 trucks. The review identified failure modes and added components necessary for safe system design.

Acknowledgements

This work was supported by the U.S. Department of Energy's Office of Energy Efficiency and Renewable Energy, Office of Hydrogen and Fuel Cell Technologies (HFTO). Dr. Zeric Hulvey of HFTO was the Technology Development Manager for this study. Argonne National Laboratory, a U.S. Department of Energy Office of Science laboratory, is operated by UChicago Argonne, LLC, under Contract No. DE-AC02-06CH11357. Lawrence Livermore National Laboratory is operated by Lawrence Livermore National Security, LLC, for the U.S. Department of Energy, National Nuclear Security Administration under Contract DE-AC52-07NA27344. Sandia National Laboratories is a multi-mission laboratory managed and operated by National Technology and Engineering Solutions of Sandia, LLC., a wholly owned subsidiary of Honeywell International, Inc., for the U.S. Department of Energy's National Nuclear Security Administration under contract DE-NA-0003525.

References

[1] W. Peschka, Liquid hydrogen: fuel of the future, Springer Science & Business Media, 2012.

[2] W. Peschka, "The status of handling and storage techniques for liquid hydrogen in motor vehicles," *International journal of hydrogen energy,* vol. 12, p. 753–764, 1987.

[3] K. Pehr, S. Burckhardt, J. Koppi, T. Korn and P. Partsch, "Hydrogen—the fuel of the future—The BMW 750hl," *ATZ worldwide,* vol. 104, p. 6–9, 2002.

[4] F. Amaseder and G. Krainz, "Liquid hydrogen storage systems developed and manufactured for the first time for customer cars," SAE Technical Paper 2006-01-0432, 2006.

[5] G. D. Berry and S. M. Aceves, "The case for hydrogen in a carbon constrained world," *Journal of Energy Resources Technology,* vol. 127, no. 2, pp. 89-94, 2005.

[6] A. Ciancia, G. Pede, M. Brighigna and V. Perrone, "Compressed hydrogen fuelled vehicles: reasons of a choice and developments in ENEA," *International journal of hydrogen energy,* vol. 21, p. 397–406, 1996.

[7] S. M. Aceves, F. Espinosa-Loza, E. Ledesma-Orozco, T. O. Ross, A. H. Weisberg, T. C. Brunner and O. Kircher, "High-density automotive hydrogen storage with cryogenic capable pressure vessels," *International Journal of Hydrogen Energy,* vol. 35, p. 1219–1226, 2010.

[8] J. Kast, R. Vijayagopal, J. J. Gangloff Jr and J. Marcinkoski, "Clean commercial transportation: Medium and heavy duty fuel cell electric trucks," *International Journal of Hydrogen Energy,* vol. 42, p. 4508–4517, 2017.

[9] H. Kang and S. Y. Kim, "Thermal design analysis of a 1 L cryogenic liquid hydrogen tank for an unmanned aerial vehicle," *International Journal of Hydrogen Energy,* vol. 39, no. 35, pp. 20009-20016, 2014.

[10] D. Verstraete, P. Hendrick, P. Pilidis and K. Ramsden, "Hydrogen fuel tanks for subsonic transport aircraft," *International Journal of Hydrogen Energy,* vol. 35, no. 20, pp. 11085-11098, 2010.

[11] W. Xu, Q. Li and M. Huang, "Design and analysis of liquid hydrogen storage tank for high-altitude long-endurance remotely-operated aircraft," *International Journal of Hydrogen Energy,* vol. 40, no. 46, pp. 16578-16586, 2015.

[12] J-K Peng et al., *Liquid Hydrogen Storage System for Heavy Duty Trucks: capacity, dormancy, refueling, and discharge,* In preparation for submission.

[13] United States Department of Energy, *Economic and National Security Impacts under a Hydraulic Fracturing Ban - Report to the President,* U.S. Department of Energy, 2021.

[14] S. Pfoser, O. Schauer and Y. Costa, "Acceptance of LNG as an alternative fuel: Determinants and policy implications," *Energy Policy,* vol. 120, p. 259–267, 2018.

[15] I. Smajla, D. Karasalihović Sedlar, B. Drljača and L. Jukić, "Fuel switch to LNG in heavy truck traffic," *Energies,* vol. 12, p. 515, 2019.

[16] C. Misra, C. Ruehl, J. Collins, D. Chernich and J. Herner, "In-use NOx emissions from diesel and liquefied natural gas refuse trucks equipped with SCR and TWC, respectively," *Environmental science & technology,* vol. 51, p. 6981–6989, 2017.

[17] "Alternative Fueling Station Locator. 2022. Available online," U.S. Department of Energy, 2022. [Online]. Available: https://www.afdc.energy.gov/stations/#/find/nearest.

[18] Y. Li, W. Li, Y. Yu and L. Bao, "Planning of LNG filling stations for road freight: a case study of Shenzhen," *Transportation research procedia,* vol. 25, p. 4580–4588, 2017.

[19] Fuel Cell Technologies Office in U.S. Department of Energy, "Multi-Year Reserach, Development, and Demonstration Plan," 2017. [Online]. Available: https://www.energy.gov/sites/default/files/2017/05/f34/fcto_myrdd_fuel_cells.pdf.

[20] M. Ferrera, "Highly efficient natural gas engines," SAE Technical Paper 2017-24-0059, 2017.

[21] P. E. Tomasz Wlodek MSc, "SAFETY ASPECTS OF DIFFERENT COMPOSITION LIQUEFIED NATURAL GAS STORAGE PROCESSES.," *International Multidisciplinary Scientific GeoConference: SGEM,* vol. 4, p. 167–174, 2016.

[22] S. Verhelst, "Recent progress in the use of hydrogen as a fuel for internal combustion engines," *International Journal of Hydrogen Energy,* vol. 39, no. 2, pp. 1071-1085, 2014.

[23] *ABAQUS 2017,* Dassault Systemes Simulia Corporation.

[24] Z. Liu, Y. Feng, G. Lei and Y. Li, "Fluid sloshing dynamic performance in a liquid hydrogen tank," *International Journal of Hydrogen Energy,* vol. 44, no. 26, pp. 13885-13894, 2019.

[25] J. Adams, C. Houchins and R. Ahluwalia, "Onboard Type IV Compressed Hydrogen Storage Systems--Cost and Performance Status 2019," *DOE Hydrogen and Fuel Cells Program Record 19008,* 2019.

[26] R. Ahluwalia, T. Hua, J.-K. Peng, S. Lasher, K. McKenney, J. Sinha and M. Gardiner, "Technical assessment of cryo-compressed hydrogen storage tank systems for automotive applications," *International journal of hydrogen energy,* vol. 35, pp. 4171-4184, 2010.

[27] G. Kaiser, D. K. Jürgen and D. B. Armin, "Pumpe für kryogene Flüssigkeiten". Germany Patent DE102008011456B4, 30 July 2021.

[28] J. Marcinkoski, "Hydrogen Class 8 Long Haul Truck Targets," *DOE Program Record 19006,* 2019.

[29] A. R. Baird, E. Hecht, B. D. Ehrhart, A. Muna and G. Bran-Anleu, "Liquid Hydrogen Heavy-Duty Vehicle Safety Review and Refueling Facility Design," Sandia National Laboratory (SAND2022-11745), 2022. [Online]. Available: https://www.osti.gov/servlets/purl/1885100.

[30] SAE J2343 Recommended Practice for LNG Medium and Heavy-Duty Powered Vehicles, SAE International, 2018.

[31] SAE J2578 Recommended Practice for General Fuel Cell Vehicle Safety, SEA International, 2014.

[32] SAE J2579 Standard for Fuel Systems in Fuel Cell and Other Hydrogen Vehicles, SAE International, 2018.

[33] NFPA 52 Vehicular Natural Gas Fuel Systems Code, National Fire Protection Association, 2019.

[34] ASME, *Boiler & Pressure Vessel Code,* American Society of Mechanical Engineers, 2019.

[35] A. R. Nerheim, V. Æsøy and F. T. Holmeset, "Hydrogen as a Maritime Fuel–Can Experiences with LNG Be Transferred to Hydrogen Systems?," *Journal of Marine Science and Engineering,* vol. 9, p. 743, 2021.

[36] E. W. Lemmon, I. H. Bell, M. L. Huber and M. O. McLinden, "NIST Standard Reference Database 23: Reference Fluid Thermodynamic and Transport Properties-REFPROP, Version 10.0, National Institute of Standards and Technology," *Standard Reference Data Program, Gaithersburg,* 2018.

[37] F. R. Schwartzberg, "Cryogenic Materials Data Handbook," 1970.

Table 1. Key physical properties for LNG and LH_2 affecting utilization onboard heavy-duty trucks [35] [36].

Physical parameter	**LNG**	**LH_2**
Molecular weight, g/mol	16.5–18.9	2
Boiling temperature at 1 atmosphere, °C	-163 to -161	-253
Heat of vaporization at 1 atmosphere, kJ/kg	442	371
Density, saturated liquid at 1 atmosphere, kg/m^3	453	71
Higher heating value, kWh/kg	54	142
Lower heating value, kWh/kg	50	120
Energy density, saturated liquid at 1 atm., kWh/L	22.5	8.520
Minimum ignition energy, mJ	0.28	0.02
Maximum laminar flame speed in air, m/s	0.374	2.933
CO2 emissions during utilization, kg/kg	2.7-2.8	0

Table 2. Packaging options for LH_2 storage for heavy duty trucks. The last two columns list internal volume per vessel with two thicknesses of MLI. These values can be multiplied by the number of vessels to calculate the total capacity for the configuration.

Configuration	Position on vehicle	Number of vessels	Diameter, cm	Length, cm	Internal Volume, L	
					MLI 11mm	MLI 21 mm
1	RM	4	30	246	125	107
2	RM, BTC	4	41	203	195	174
3	RM	4	41	246	243	216
4	FM	2	53	120	172	159
5	FM	2	53	152	233	215
6	FM, BTC	2	53	203	331	304
7	FM	2	66	152	360	339
8	FM	2	66	203	515	484
9	FM	2	66	229	594	557
10	FM	2	66	305	824	770

Table 3. Material properties [34] [37]

Property / Material	σ_u	σ_y	E	$\sigma_{a,\ MPa}$		Density
	MPa	MPa	GPa	RT	-195	g/cc
Al 2219-T87	454	344	70	129.7	196.9	2.84
Al 5083-O	276	124	70	78.8	107	2.66
SS 304, 316	515	205	200	137	243	8.0

Table 4. Thickness and mass of the shell with and without a stiffening ring

	Thickness, mm		Weight, kg
	Cylinder	Dome	
Without stiffening ring	5.8	2.9	99.4
With stiffening ring	4.5	2.9	78

Table 5. Thicknesses and mass of the liner made of different materials

Material \ Liner	Thickness, mm		Weight, kg
	Cylinder	Dome	
Al 2219-T87	2.7	2.9 (junction) 4.5 (port)	44
Al 5083-O	4.4	5.2 (junction) 8 (port)	74
SS 304, 316	2.6	2.8 (junction) 4 (port)	126

Table 6 Summary of projected system cost, mass, and capacity for multiple medium and heavy-duty vehicle on-board LH2 storage configurations. Costs are projected to 100,000 systems per year and reported in 2016$.

Configuration	Position on Vehicle	Number of Tanks	Projected Cost ($/kg usable H2)	Projected Empty Mass (kg/system)	Projected Capacity (Usable kgH2/system)	Projected Cost ($/kg usable H2)	Projected Empty Mass (kg/system)	Projected Capacity (Usable kgH2/system)
			11 mm MLI			21 mm MLI		
Config 1	RM	4	$898	271	20.8	$813	276	23.9
Config 2	RM, BTC	4	$528	302	36.4	$507	308	39.8
Config 3	RM	4	$435	345	45.6	$425	354	49.3
Config 4	FM	2	$736	196	16.6	$697	199	18.2
Config 5	FM	2	$544	215	23.0	$529	218	24.7
Config 6	FM, BTC	2	$392	246	33.1	$391	254	34.9
Config 7	FM	2	$353	251	37.0	$351	256	39.1
Config 8	FM	2	$255	294	53.6	$260	301	55.9
Config 9	FM	2	$226	317	62.0	$232	325	64.5
Config 10	FM	2	$174	397	86.8	$183	408	89.1

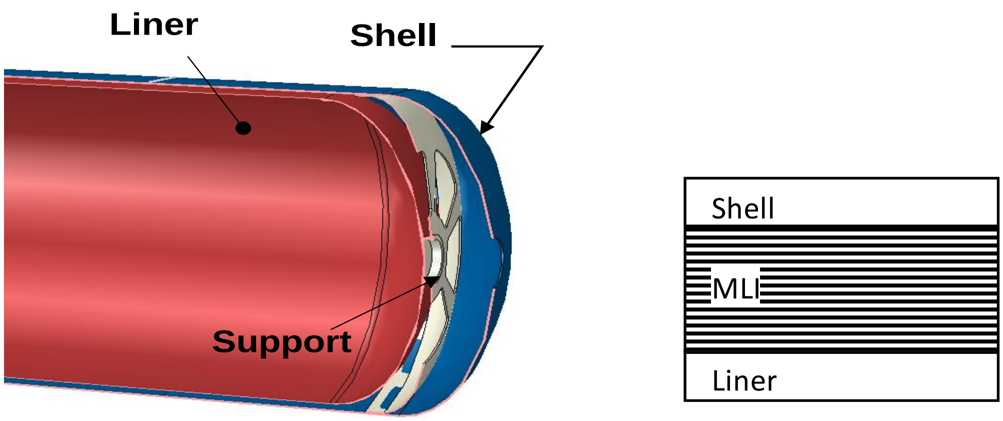

(a) (b)

Fig. 1 (a) Section view of the LH2 vessel, (b) location of MLI between the inner liner and the outer shell

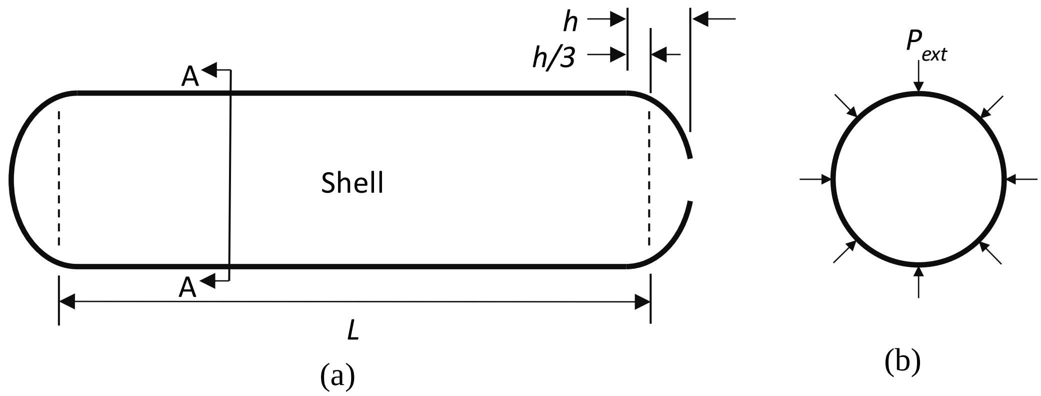

Fig. 2 (a) Design length of a shell between lines of supports (b) Section A-A showing external pressure exerted on the shell

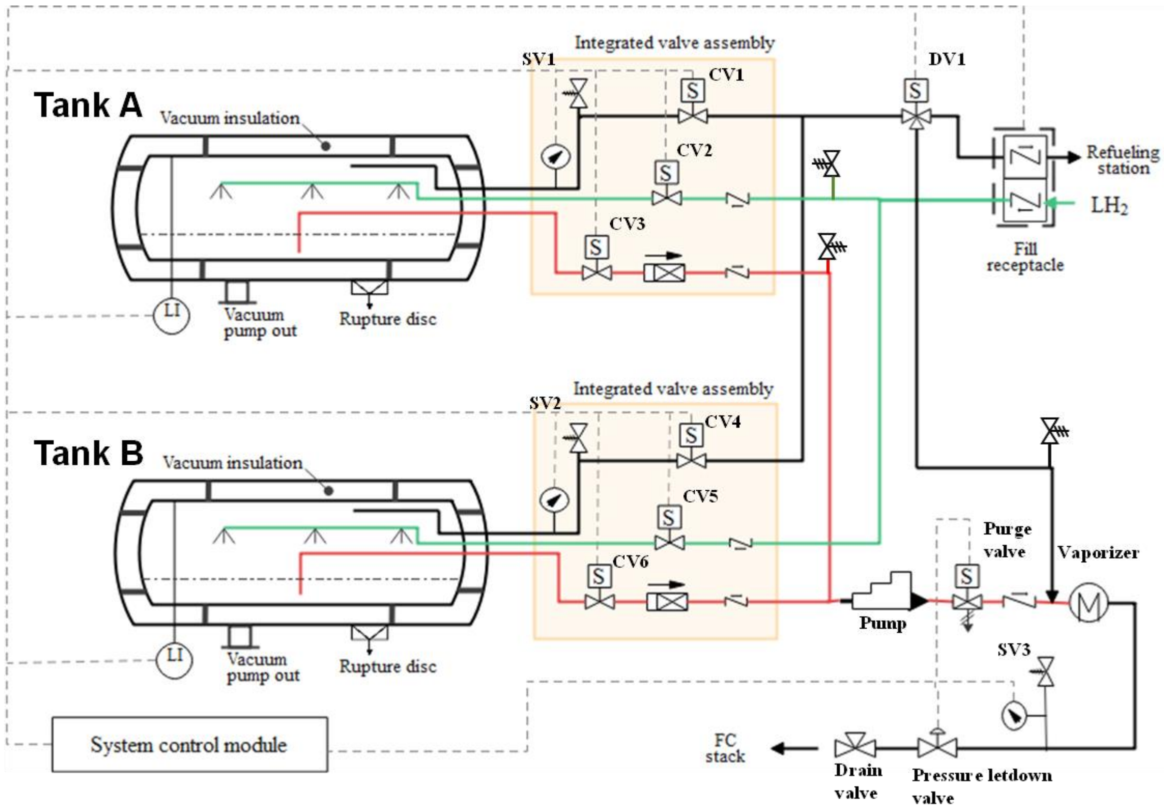

Fig. 3 Hydrogen fuel system with LH_2 pump onboard the truck

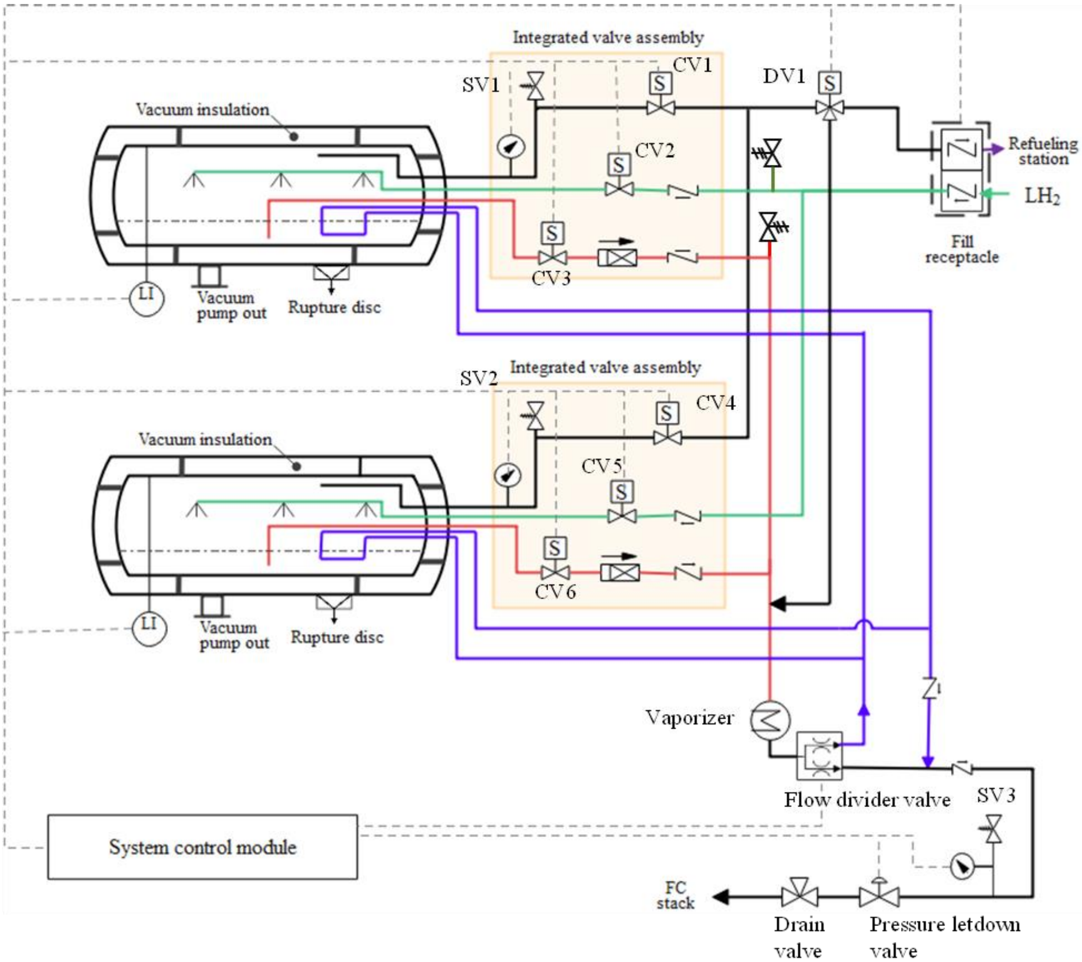

Fig. 4 Hydrogen fuel system without a LH_2 pump onboard the truck

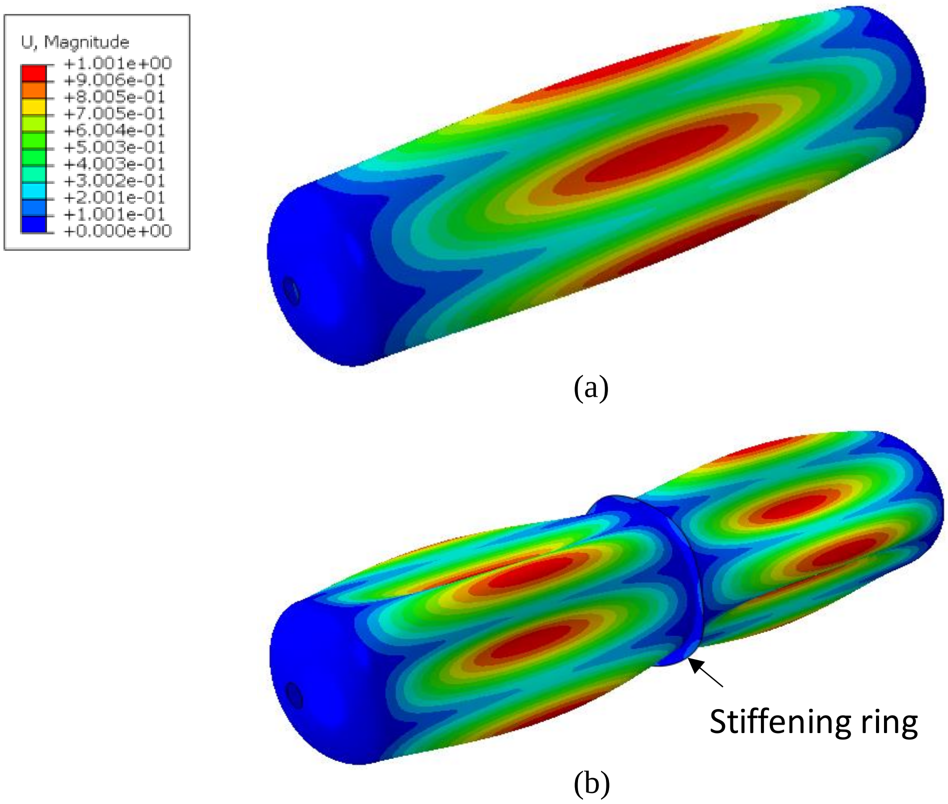

Fig. 5 The first bucking mode (displacement, U in mm) of a LH_2 vessel with external pressure. (a) without a stiffening ring, (b) with a stiffening ring.

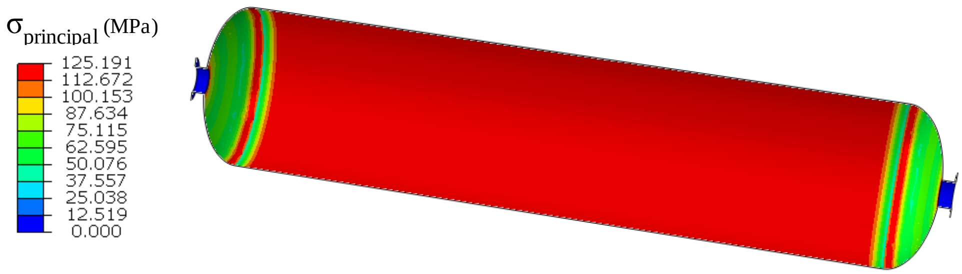

Fig. 6 Principal stresses on Al 2219-T87 liner (σ_a = 129.7 MPa)

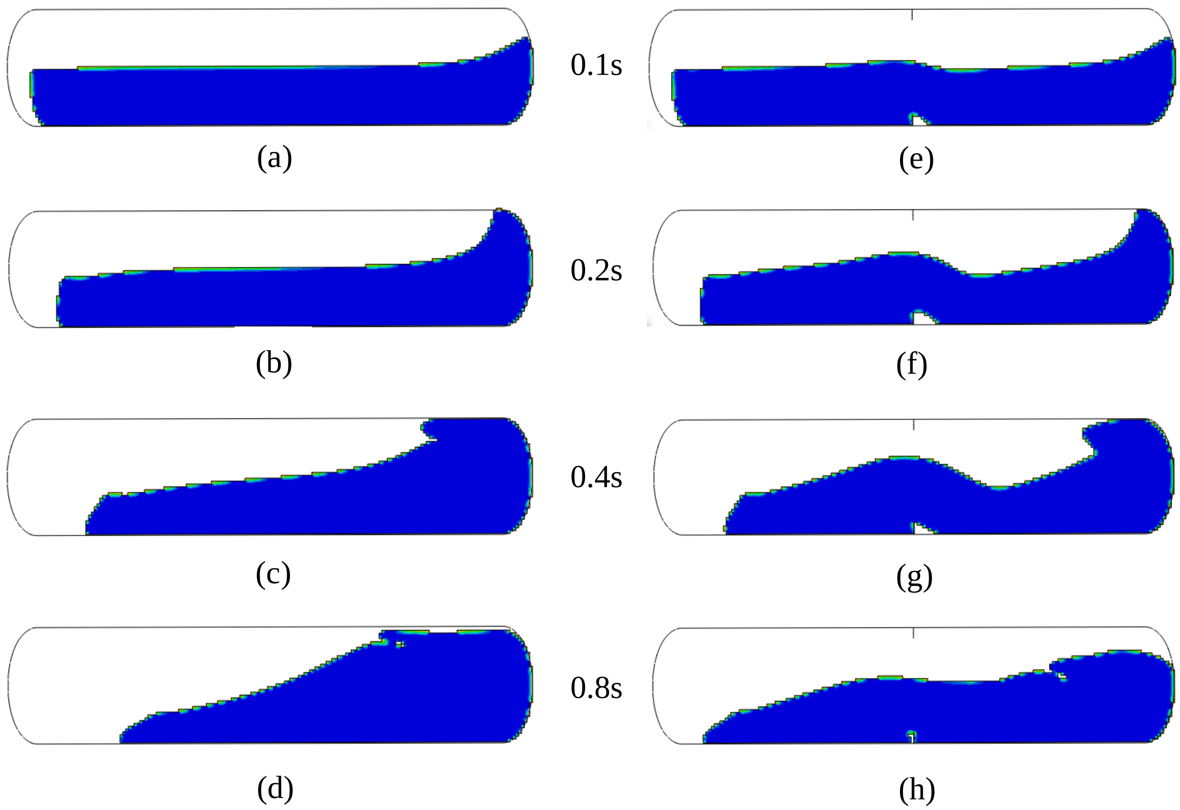

Fig. 7 LH_2 sloshing in a half-filled vessel without (a-d) and with (e-h) a baffle at different times during and following a sudden 2G deceleration starting at t=0 and ending at t=0.1 s (initial velocity 2 m/s)

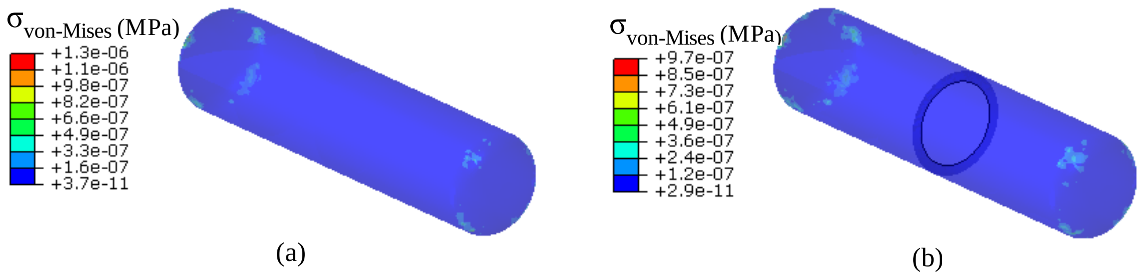

Fig. 8 Stress distributions due to deceleration and sloshing over a half-filled vessel without (a) and with (b) a baffle at t = 0.1 s (the moment when the truck stops) during a 2G deceleration starting with the truck moving at 2 m/s

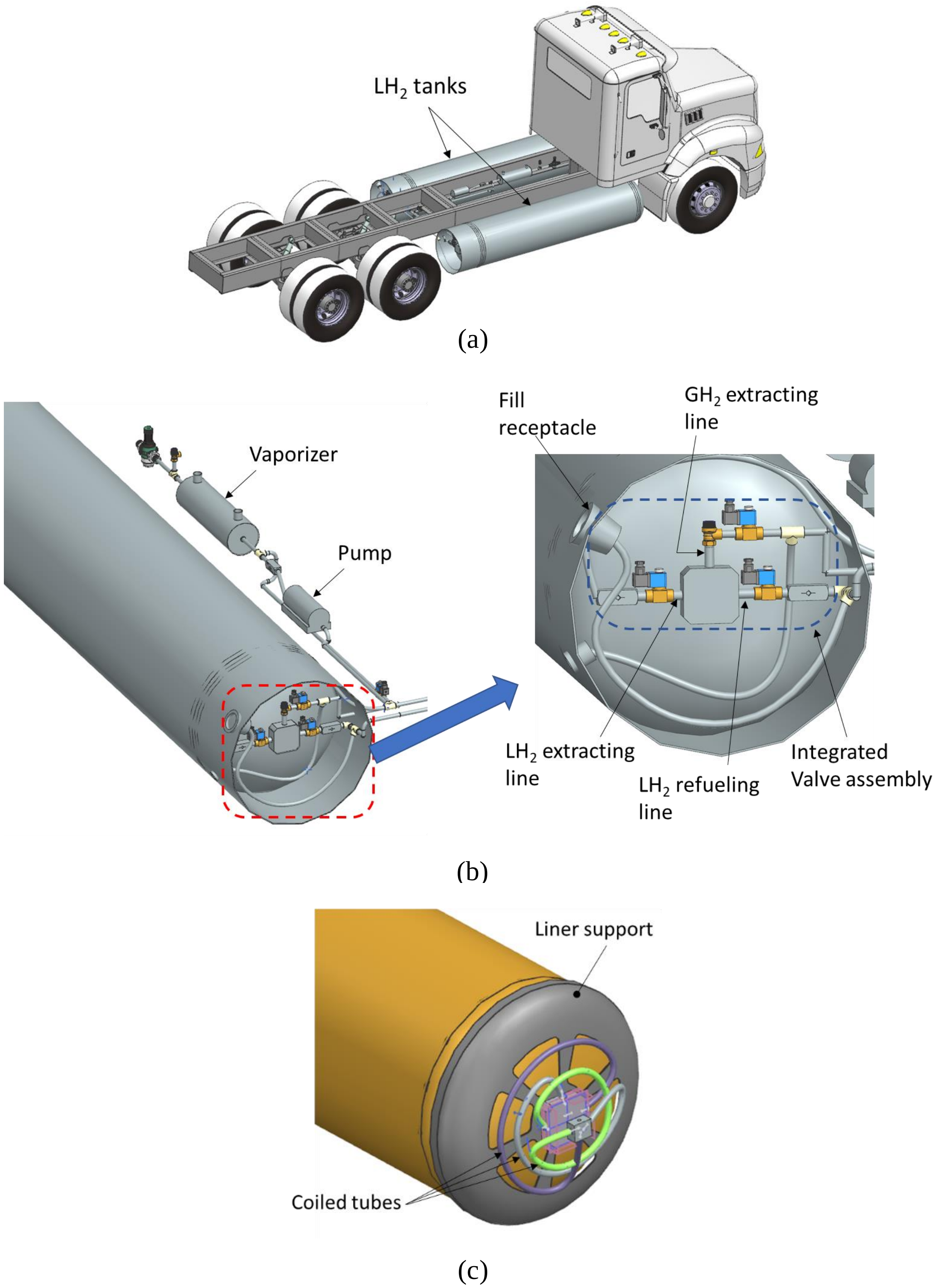

Fig. 9 LH_2 fuel system conceptualization: (a) frame-mounted dual tank system (b) LH_2 tank and BOPs (c) Coiled tubes

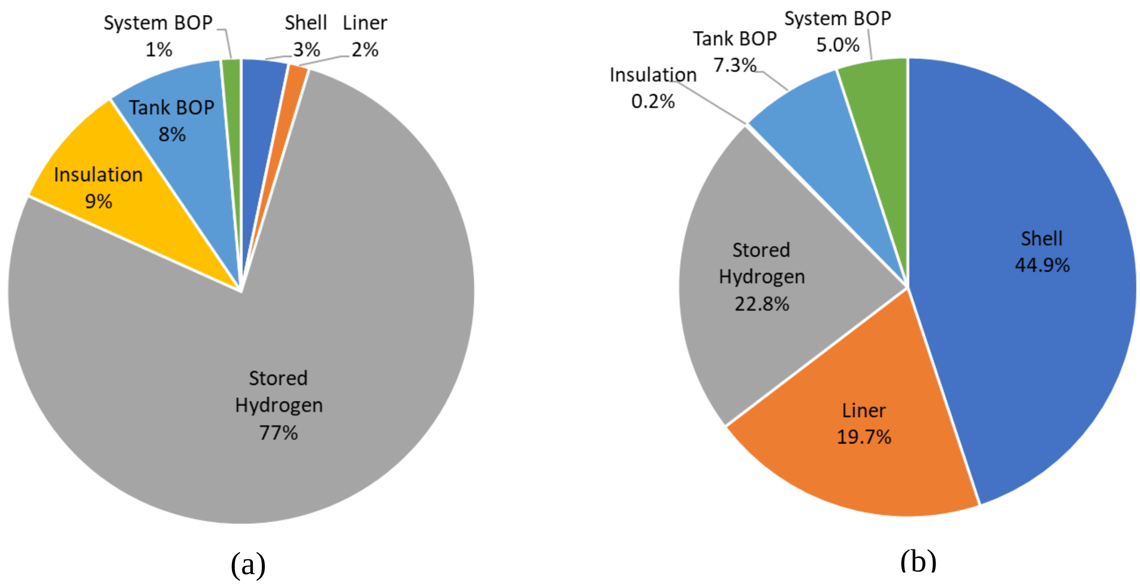

Fig. 10 LH_2 storage system performance: (a) volume distribution, (b) weight distribution. (It is noted that 22.8% weight fraction represents total stored hydrogen onboard the vessel, not to be confused with 19.6% usable LH_2 weight fraction cited elsewhere in the paper.)

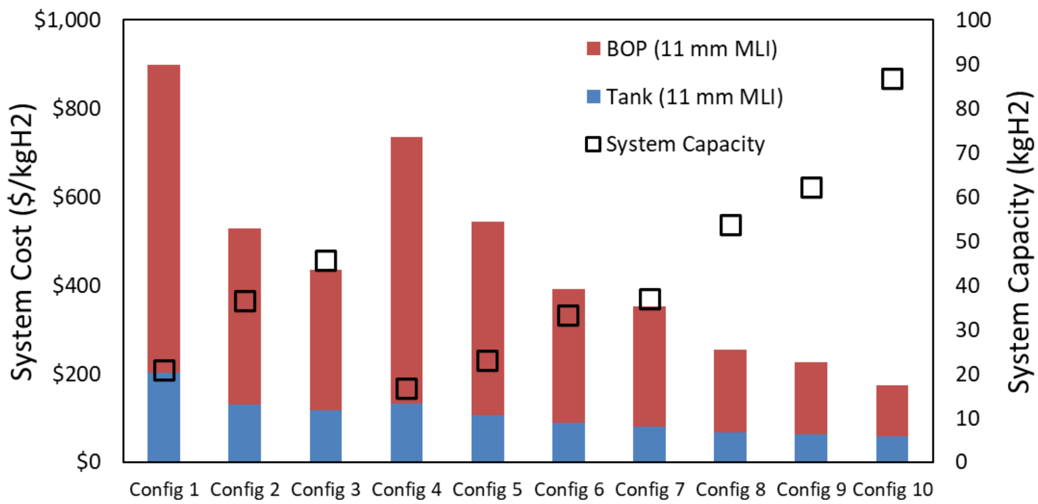

(a)

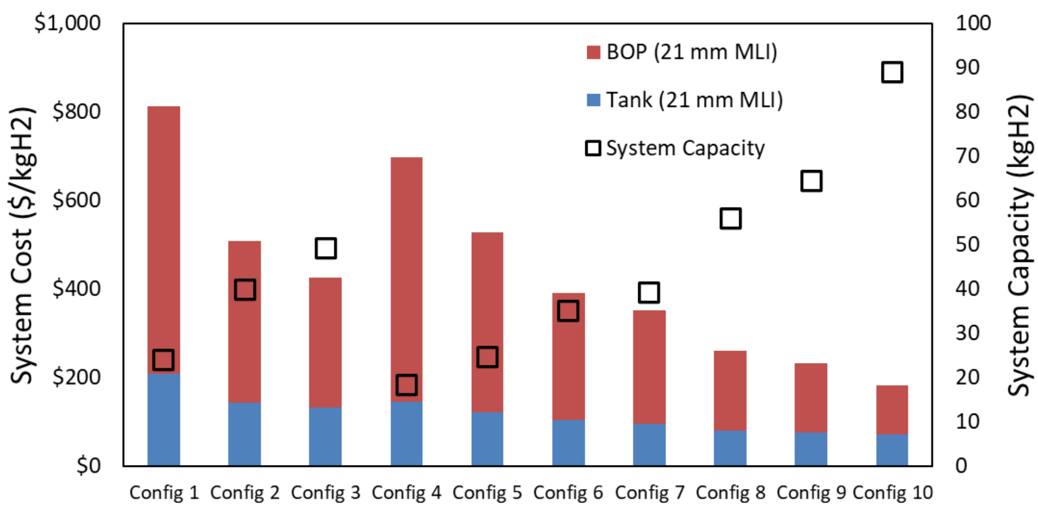

(b)

Fig. 11 Cost breakdowns for multiple LH_2 storage system configurations from Table 2 showing vacuum jacketed vessel cost and balance of plant cost contributions. Manufacturing costs are projected to 100,000 systems per year and reported in 2016$. Top and bottom figures show cost breakdowns for systems with (a) 11 mm and (b) 21 mm MLI, respectively. System capacity represents total values for all vessels in the selected configuration and is based on usable hydrogen mass.

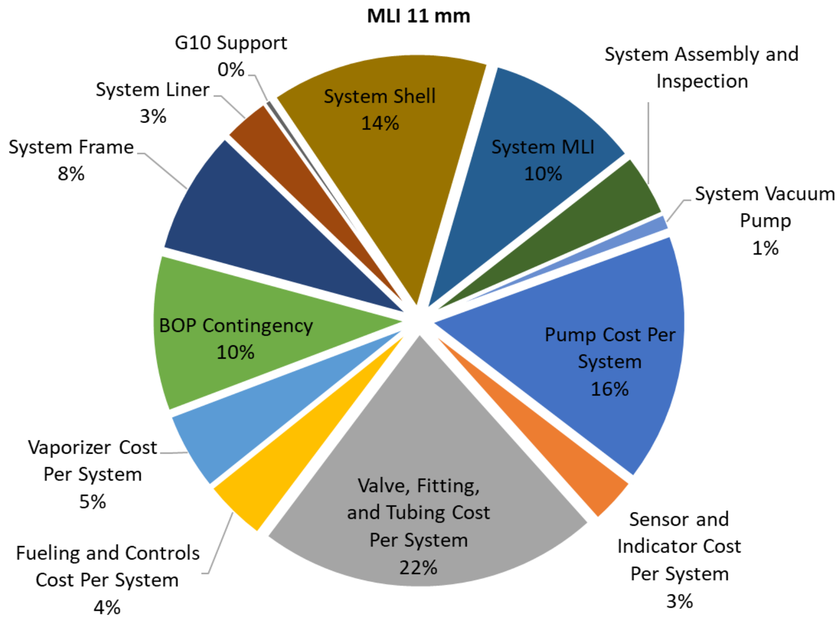

(a)

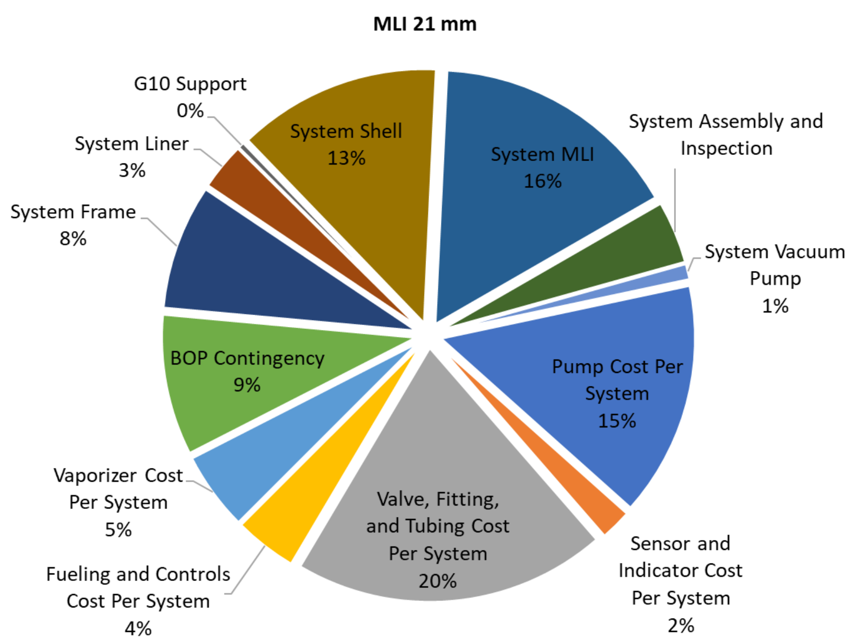

(b)

Fig. 12 Cost breakdown for configuration 10 (frame-mounted two-vessel system) with (a) 11 mm and (b) 21 mm MLI, respectively. Manufacturing cost is projected to 100,000 systems per year and expressed in 2016$. Vessel cost categories (liner, insulation, shell, etc.) are shown as expanded slices to contrast with balance of plant and frame items.

Abbreviations

BOP: Balance of plant

BTC: Behind the cab

CNG: Compressed natural gas

DBTT: Ductile-to-brittle transition temperature

FE: Finite element

FM: Frame mounted

FMEA: Failure modes and effects analysis

GH_2: Gaseous hydrogen

LH_2: Liquid hydrogen

LNG: Liquefied natural gas

MLI: Multilayer insulation

NFPA: National fire protection association

RM: Roof mounted

SCS: Safety, codes, and standards